

## RESEARCH ARTICLE OPEN ACCESS

# Studying the Impact of Impurities on the Performance of Cadmium-Free all Sputtered CIGS Solar Cells Using Titanium–Tungsten Barrier

Tanvi Upreti<sup>1,2,3</sup>  | Jan Keller<sup>2</sup>  | Lasse Vines<sup>4</sup> | Muhammad Israr-Qadir<sup>1</sup>  | Esko Niemi<sup>1,3</sup>  | Marika Edoff<sup>2,3</sup>

<sup>1</sup>Midsummer AB, Järfälla, Sweden | <sup>2</sup>Ångström Laboratory, Division of Solar Cell Technology, Uppsala University, Uppsala, Sweden | <sup>3</sup>Wallenberg Initiative Materials Science for Sustainability, Ångström Laboratory, Division of Solar Cell Technology, Uppsala University, Uppsala, Sweden |

<sup>4</sup>Department of Physics, Centre for Materials Science and Nanotechnology, University of Oslo, Oslo, Norway

**Correspondence:** Tanvi Upreti (Tanvi.upreti@midsummer.se)

**Received:** 19 June 2025 | **Revised:** 20 October 2025 | **Accepted:** 23 October 2025

**Funding:** Knut and Alice Wallenberg Foundation

**Keywords:** all-sputtered Cu(In, Ga)Se<sub>2</sub> | cadmium free | diffusion | simulations | steel substrates | titanium/tungsten

## ABSTRACT

Midsummer AB specializes in producing flexible, lightweight, cadmium-free, all-sputtered Cu(In, Ga)Se<sub>2</sub> (CIGS) modules on steel substrates. This study investigates the role of a titanium/tungsten (TiW) barrier layer, placed between the steel substrate and the back contact, in controlling the diffusion of three major impurities—iron (Fe), chromium (Cr), and nickel (Ni)—which are believed to be detrimental to CIGS devices. For a device with a 64 nm barrier layer, an efficiency of 14% is obtained, limited by a reduced fill factor (FF) and low open-circuit voltage ( $V_{OC}$ ). Increasing the thickness of the barrier layer to 128 nm leads to improvements in both  $V_{OC}$  and FF, yielding an efficiency of 16%. This finding is supported by secondary ion mass spectrometry measurements, which show lower impurity levels for thicker barriers. The results indicate that impurity diffusion into the CIGS layer during deposition significantly affects device performance, but this can be mitigated using TiW barrier layers. Glow discharge optical emission spectroscopy is employed to examine the in-depth compositional profile of the CIGS layer. Additionally, a solar cell capacitance simulator (SCAPS-1D) is used to assess the impact of impurities on performance and compare the results with experimental data.

## 1 | Introduction

Thin film photovoltaic technologies, particularly Cu(In, Ga)Se<sub>2</sub> (CIGS), have unique properties for building integration (BIPV). With a simplified production process and easy availability of raw materials along with its comparable commercial viability, flexibility and stability, it is emerging as a promising commercial photovoltaic technology [1, 2] for BIPV compared to crystalline silicon technology. A range of materials (rigid ceramic, metal or flexible polymer) can be used as a substrate material. Recently, a group from Uppsala university produced a Ag-alloyed CIGS solar cell on glass with an impressive

performance of  $\approx 23.6\%$  [3] and another group from EMPA reportedly developed 21.38% CIGS on polyimide flexible substrate [4]. Miasolé produced CIGS modules on flexible steel substrates with an efficiency of 17.1% [5]. Not flexible but a light-weight glass-based large area CuIn<sub>1-x</sub>Ga<sub>x</sub>Se<sub>2-y</sub>S<sub>y</sub> (CIGS) module produced by Avancis gave an impressive efficiency of 20.3% [6]. For flexible lightweight photovoltaics, stainless steel (SS) foil is a preferred substrate. This is mainly due to easy availability, matching thermal expansion coefficient of steel with CIGS along with the mechanical stability (even at high temperatures), but most importantly is the low cost of the substrate material [7, 8]. With mild steel substrate Carron et al. obtained

This is an open access article under the terms of the [Creative Commons Attribution-NonCommercial](https://creativecommons.org/licenses/by-nc/4.0/) License, which permits use, distribution and reproduction in any medium, provided the original work is properly cited and is not used for commercial purposes.

© 2025 The Author(s). *Solar RRL* published by Wiley-VCH GmbH.

an efficiency of 18% at lab scale [9]. Utilizing a ferritic SS substrate, steel 1.4016 or AISI 430, Midsummer has earlier reported an efficiency of  $\approx 16.7\%$  (active area of  $192\text{ cm}^2$ ) for a cadmium-free all-sputtered solar cell. [10] Despite relatively high efficiencies, CIGS solar cells are still below their theoretical limit of  $\approx 33\%$  [11], which implies that there is still room for improvement. The first step toward bridging this gap is to understand the different loss mechanisms.

With SS as a substrate, there are two major issues which seem to be affecting the performance of these devices: (a) diffusion of impurities from the substrate [12, 13], e.g., Na in soda lime glass (SLG) substrates or metal impurities from steel substrates and (b) diffusion barriers, or stack isolation [14]. SS already has Fe, Cr, Ni, and Mn along with other detrimental materials in its composition. These materials can very easily diffuse into the absorber layer (CIGS) during high temperature processing and can adversely impact the performance of a device by creating deep level defects in the absorber layer. [13] Common oxide barriers such as  $\text{Al}_2\text{O}_3$  [15] (typically  $0.1\text{--}3\ \mu\text{m}$ ) and  $\text{SiO}_2$  [16] ( $200\text{--}1000\text{ nm}$ ), are effective in blocking the Fe and Cr impurities from steel substrates and improving device's stability [17]. Li et al. [18] in their work used TiN ( $50\text{ nm}$ ) as a barrier layer to suppress Na diffusion into the CIGS absorber layer. They could achieve a high performing device with a better stability besides an improved crystallinity and uniformity of the CIGS layer. Woo et al. [19] used a  $5\text{ nm}$  TiN barrier layer to prevent the diffusion of Se into the Mo back contact electrode and improve the efficiency of their devices. Jiang et al. [20] deposited a pure Ti film ( $200\text{ nm}$ ) through RF sputtering on a SS foil, which effectively blocked Fe and Cr during CIGS deposition process and improved the device efficiency. So far to the best of our knowledge, TiW ( $291\text{ nm}$ ) was used as an effective barrier in suppressing the Fe diffusion to the CIGS layer from a pure Fe substrate by Gao et al. [21] Though less commonly used than oxides or nitrides, its high thermal stability, low diffusivity, and good electrical conductivity makes TiW an attractive material for integrating in the CIGS device making. Besides it also has an ideal coefficient of thermal expansion, which corresponds to the Mo back contact, and is compatible with the steel substrate [21].

With SS it also becomes important to infuse adequate amounts of sodium (Na) which suppresses the bulk defects and nonradiative recombination. Adding Na enhances the quasi-fermi level splitting thus increasing the  $V_{\text{OC}}$  in the cells due to an increased p-doping of the CIGS layer, lowered hole barriers at grain boundaries, and increased hole mobility [22, 23]. A secondary impact of infusing Na is that it influences the interdiffusion of gallium (Ga) and indium (In) during CIGS deposition as Na tends to accumulate In at the grain boundary and confining Ga to the grain interiors [24]. This results in a variation in In and Ga concentrations which creates an in-depth band gap grading [25, 26].

In this paper, we present for the first time the impact of TiW (10% Titanium–90% Tungsten by weight) as a diffusion barrier layer for a Cd free all sputtered CIGS solar cell. A conductive diffusion barrier layer of TiW was sputtered at different thicknesses. Results from secondary ion mass spectrometry (SIMS) and glow-discharge optical emission spectroscopy (GDOES) are presented to study the influence of barrier thickness on

the device characteristics. jV data of the different devices were analyzed and compared with the SCAPS-1D simulation tool [27].

## 2 | Experimental Setup

The photovoltaic cells with the structure SS/TiW/MoNa ( $250\text{ nm}$ )/Mo ( $100\text{ nm}$ )/CIGS ( $900\text{ nm}$ )/ $\text{In}_2\text{S}_3$  ( $50\text{ nm}$ )/window layer ( $100\text{ nm}$ ) / TCO ( $170\text{ nm}$ ) were deposited on a ferritic stainless-steel substrate following an in-line vacuum sputtering in Midsummer's DUO CIGS solar cell sputtering tool which has 25 dc or pulsed dc magnetron sputtering stations. An alkali doped Mo is sputtered on TiW to compensate for the lack of a sodium source. For studying the optimum thickness of the diffusion barrier layer in blocking the impurities from diffusing into the CIGS absorber, TiW was sputtered at different thicknesses ( $0, 64, 74, 83, 112, 128, 208,$  and  $232\text{ nm}$ ). A standard  $208\text{ nm}$  TiW (reference) is currently used in the production line at Midsummer was also used for our study. Quaternary CIGS compound sputtering targets differing in  $[\text{Ga}]/([\text{In}]+[\text{Ga}])$  ratio were used to produce the Ga- graded CIGS profiles. Subsequently, a p–n junction was created by sputtering an n-type  $\text{In}_2\text{S}_3$  buffer layer with a small oxygen inclusion [10]. The cell was completed by depositing a resistive window layer which is a magnesium alloyed zinc oxide ( $\text{Zn}_{1-x}\text{Mg}_x\text{O}$ ). The primary function of this layer is to passivate the underlying layers (buffer and absorber layers) from the high energy particles during the deposition of the top contact. Its other function is to prevent shunting that can be caused by crystalline defects in the CIGS layer, which are very easily formed in large area cells. Finally, ITO as a transparent conductive oxide (TCO) layer forms the top contact. Unlike the resistive window layer, it is highly conductive to efficiently collect and transport the photo-generated electrons to the external circuit with minimal resistive losses. The devices were screen printed with silver (Ag) paste to prepare 8 samples with an active area of  $238.83\text{ cm}^2$ , called full cells, and 2 samples (with 196 cells each) with an active area  $196 \times 1\text{ cm}^2$ , called pixel cells. Pixelated samples were then sectioned to get multiple cells with an area of  $1\text{ cm}^2$ .

During the full solar cell deposition at Midsummer, the substrates are successively brought to different sputtering chambers (1–25) of DUO for the deposition of diffusion barrier, absorber, buffer, window, and TCO layer, all under vacuum. There is a possibility of running DUO under production mode, for bulk production, or OBO (one-by-one) mode for R&D purposes. In production mode there are 30 substrates present inside the machine simultaneously and every 18 s a finalized device (without a silver grid) is unloaded and replaced with a new substrate. A detailed description of this tool can be found in ref. [28].

The full cells were measured directly after the screen printing, using the automated jV profiler attached to the screen-printing line at Midsummer. The current voltage (jV) and external quantum efficiency (EQE) of the pixel cells were measured in two steps. First, all the samples (for all thicknesses) were tested using the MPI pixel probe station at Midsummer followed by the EQE measurement of the selective pixels, from the edge and the center giving similar jV characteristics ( $\pm 10\%$  range), using Bentham EQE equipment. The high performing pixels of each thickness were subsequently characterized using a home built jV and

EQE setup at Uppsala University. The  $jV$  was done at 25 °C with an LED-based setup used as an illumination source. EQE measurements were performed to calculate the short circuit current density ( $j_{sc}$ ) values of the best performing cells. GDA 750 HR by Spectrumba was used to perform the GDOES on our samples. Estimation of the critical impurities and quantification of their concentrations in the samples were done by SIMS using a Cameca IMS7f tool equipped with Cs and O<sub>2</sub> primary ion sources. O<sub>2</sub> primary ions were used for profiling. Absolute concentration calibrations for the observed impurities were obtained using a reference sample with known impurity content of the elements of interest. The reference sample was cut out from a badly performing CIGS target, for which the impurity levels of Fe, Cr, and Ni (along with other minor impurities) have been measured by GDMS at an external laboratory.

### 3 | Results and Discussion

To investigate the Ga and In and thus an in-depth bandgap variation of our devices, GDOES was performed on all samples. Figure 1 shows the Ga and In intensities as measured for three representative thicknesses: 0, 208 nm and an intermediate thickness of 112 nm. A detailed elemental profile for all the thicknesses, respectively, is shown in Figure S1. As observed in both the images, irrespective of the thickness of the diffusion barrier layer, a similar elemental profile for [Ga], [In], [Cu], and [Se] is obtained. A sample without TiW barrier was made in another run and therefore had a lower thickness of the CIGS layer. Figure S2 gives a comparison of Fe, Cr profile for 0, 112 nm and reference 208 nm TiW sample. For Fe, while the signal intensity in itself is low, the analysis clearly shows the primary implication of no barrier layer versus a diffusion barrier layer.

With several quaternary compound CIGS sputtering targets with different Ga/(Ga+In) ratios a graded Ga profile is obtained. The ratio between Ga and In determines the bandgap of the absorber layer and can vary from 1 eV for pure CuInSe<sub>2</sub> (CIS) to 1.7 eV for

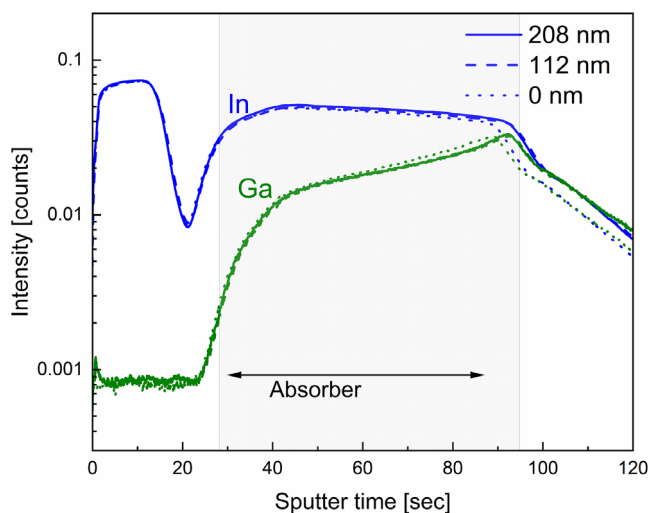
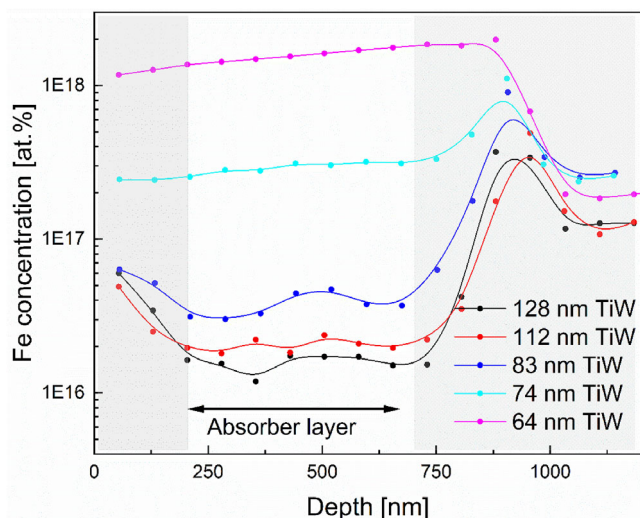


**FIGURE 1** | In and Ga intensity for three different thicknesses of TiW (208, 112, and 0 nm) measured through GDOES on SS/TiW/MoNa/Mo/CIGS/In<sub>2</sub>S<sub>3</sub>/window layer sample. The 208 nm TiW is the diffusion barrier layer thickness used in the production process at Midsummer.

pure CGS. The interface between CIGS and the back contact, from Figure S1, shows the Ga-grading extending all through the CIGS layer, which is obtained by depositing CuGaSe<sub>2</sub> (CGS) from the first target and then CIGS from targets with lower and lower [Ga]/([In]+[Ga]) ratio. The influence of such graded compositional profiles on key electrical parameters, such as open-circuit voltage ( $V_{oc}$ ) and short-circuit current ( $j_{sc}$ ), is well established in the literature [29–34], where they are shown to enhance carrier collection efficiency and suppress recombination losses at the rear contact. Since the bandgap varies as a function of the depth of the CIGS absorber, an effective bandgap is calculated. For our samples, a bandgap of 1.08 was calculated from the absorption edge of the EQE spectrum, 90% of the SS is made up of Fe, Cr, Ni, and Mg, while the remaining 10% consists of the minor alloying elements and impurities optimized for mechanical and chemical stability. Thus, the substrate itself acts as a source of impurities which can diffuse to the CIGS layer above 500 °C. When ferritic steel substrates are concerned, Fe, Cr, and Ni have been investigated as detrimental impurities by different groups. Fe, which is highly studied, is considered to be the most harmful impurity [13, 25, 35]. Ma et al.<sup>37</sup> in their study used Cu sources with different purity to evaporate the CIGS layer. They found that even a trace composition of 0.03% Fe impurity reduced the efficiency of their devices from 18% to 14%. Wuerz et al. [25] estimated a tolerable limit of 0.08 ppm Fe for a high efficiency CIGS device ( $\approx 20\%$ ) while for a low efficiency device it was found to be 1 ppm. The overall consensus of all the studies is however the same that Fe is indeed a detrimental impurity as it can easily diffuse from the steel substrate into the CIGS absorber layer [25, 35, 36] create nonradiative recombination centers which reduces the charge carrier lifetime [37], and consequently degrades the efficiency of a device.

Unlike Fe, the impact of Cr and Ni is more nuanced as there doesn't seem to be a consensus on treating them an impurity impacting the performance of a solar cell. Some groups have used Cr as a barrier layer to prevent Fe diffusion to the CIGS absorber layer [35, 38, 39]. However, under high temperature processing Cr itself starts diffusing to the CIGS layer thereby acting as an impurity and starts hindering the device's performance [15, 40]. Pianezzi et al. observed a reduction of almost 23% for a Cr concentration of 0.22 at%. [40] Ni was used as barrier layer to prevent the diffusion of excess Cu from the substrate into CIGS by Rechid et al. [41]. They observed a steep decrease in the grain size which was attributed to Ni accumulating at the CIGS/Mo interface, but the overall impact of Ni was termed to be non-detrimental. However, Jackson et al. [42] in their study termed Ni to be a notorious impurity, even for their small concentration. This was confirmed also by Pianezzi et al. [40] who observed an efficiency loss of 83% with a 0.26 at% of Ni impurity in CIGS layer. These studies suggest that both Ni and Cr also degrade the electronic properties by creating deep level traps and recombination centers, thereby negatively impacting the devices' performance.

For obtaining the concentration of these impurities,  $2 \times 2$  cm<sup>2</sup> samples were cut out from a 238.8 cm<sup>2</sup> CIGS wafer for selected TiW thicknesses. SIMS measurements were done on these two samples—labeled as edge and center respectively for the selected thicknesses. Due to high variability and absence of a systematic trend in the edge profiles, we have shown only the center profiles.



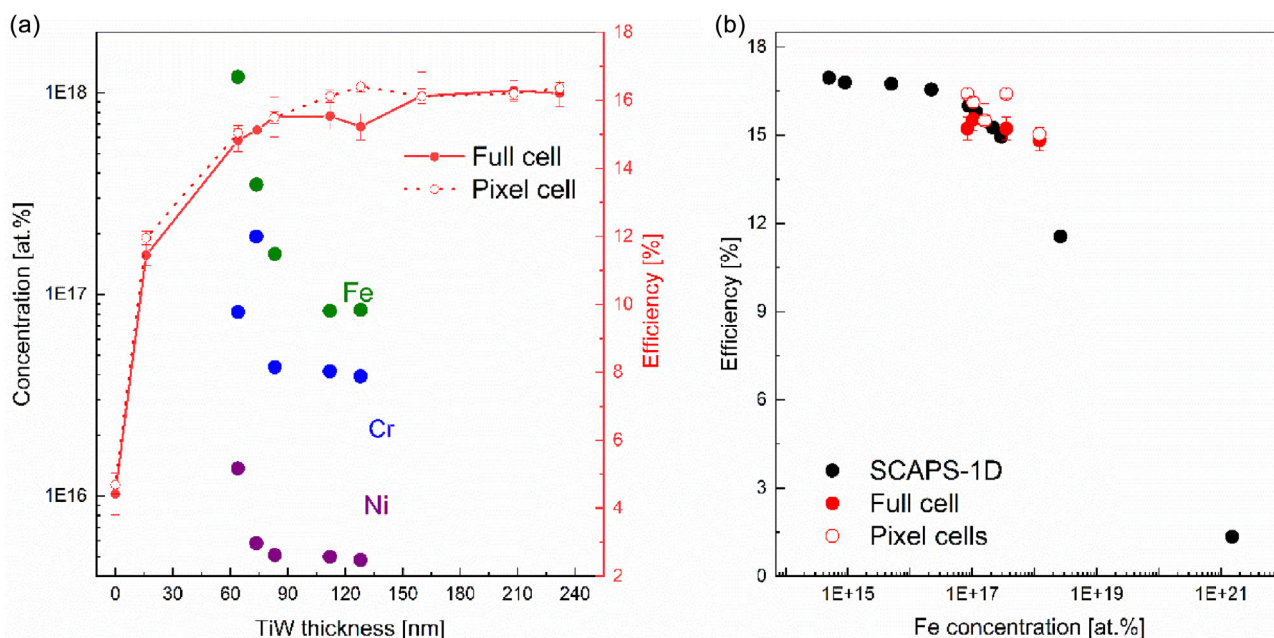
**FIGURE 2** | Fe concentration in CIGS cell obtained through SIMS measured at the center shows decreasing diffusion of the impurity with increasing thickness of the barrier layer (128, 112, 83, 74, and 64 nm).

Figure 2 shows the concentration of Fe diffusing into the CIGS layer, when measured at the center, for the selected samples. The result shows that for a 64 nm thick TiW layer, the concentration of Fe diffusing into the absorber layer is  $1.5 \times 10^{18}$  atoms  $\text{cm}^{-3}$ . As the thickness of the barrier layer is increased, the concentration of Fe diffusing into the absorber layer decreases and for thicknesses beyond 74 nm the concentration of Fe is substantially reduced. For a no barrier sample (0 nm TiW), it is thus implicit that the concentration of the impurities, here Fe, diffusing into the absorber region will be significantly higher compared to 64 nm TiW. Since the Fe concentration has already started to

level off beyond 112 nm, we do not expect orders of magnitude difference in the Fe concentration for 208 and 232 nm TiW.

In these selected samples, we observed a consistent higher concentration of Fe in the absorber layer with Cr as the next highest impurity concentration compared to Ni (Figure S3). The high concentration of the Fe can partially be attributed to the Fe impurities from the sputtering targets used in the DUO tool. The impact of these trace impurities on the efficiency of CIGS solar cells is illustrated in Figure 3a, which shows the efficiency of full cell (238.8  $\text{cm}^2$ ) and pixel CIGS cells measured at Midsummer (red symbols) together with the measured concentration of Fe, Cr, and Ni versus TiW thickness. Figure 3b compares the simulated efficiency values from SCAPS-1D (black symbols) as a function of the Fe concentration varied over a range to account for all the barrier thicknesses with the corresponding experimental full cell and pixel cell efficiency. While we observe a low concentration of Ni for all the TiW thicknesses, the impact of such low concentrations of Ni has not been studied in great details for CIGS. However, given that the Mo target also contains Ni as an impurity, as high as 10 ppm, the observed small concentration of Ni indicates the effectiveness of the TiW barrier layer in controlling the diffusion of the impurities.

jV curves for different thicknesses of TiW are shown in Figure S4 measured at AM 1.5 at 1 sun. The EQE of these devices are shown in Figure S5. The mismatch between  $J_{SC, jV}$  and  $J_{SC, EQE}$ , due to the light source used for the jV measurements, is corrected by multiplying the  $J_{SC, jV}$  with the correction factor,  $J_{SC, EQE}/J_{SC, jV}$  for calculating the efficiency ( $\eta_{EQE}$ ). The corrected jV-curves of CIGS solar cells with varying diffusion barrier thickness (TiW) are shown in Figure 4 below. From Figure 4a, a clear trend in the improvement of open circuit voltage ( $V_{OC}$ ) and fill



**FIGURE 3** | (a) Correlation between the efficiency (median) of full (238.8  $\text{cm}^2$ ) and pixelated CIGS cells with error bars denoting the standard deviation in measurements over the range of samples measured at Midsummer and concentration of Fe, Ni, and Cr in CIGS cells as obtained via SIMS for different diffusion barrier layer thickness. (b) Comparison of the full (238.8  $\text{cm}^2$ ) and pixelated cell's efficiency of CIGS solar cell as obtained experimentally and efficiency obtained via SCAPS-1D simulations. For simulations, Fe concentration was varied between  $5 \times 10^{14}$  and  $1.5 \times 10^{21}$  at% to account for the entire range of TiW thickness and to obtain the corresponding efficiency values.

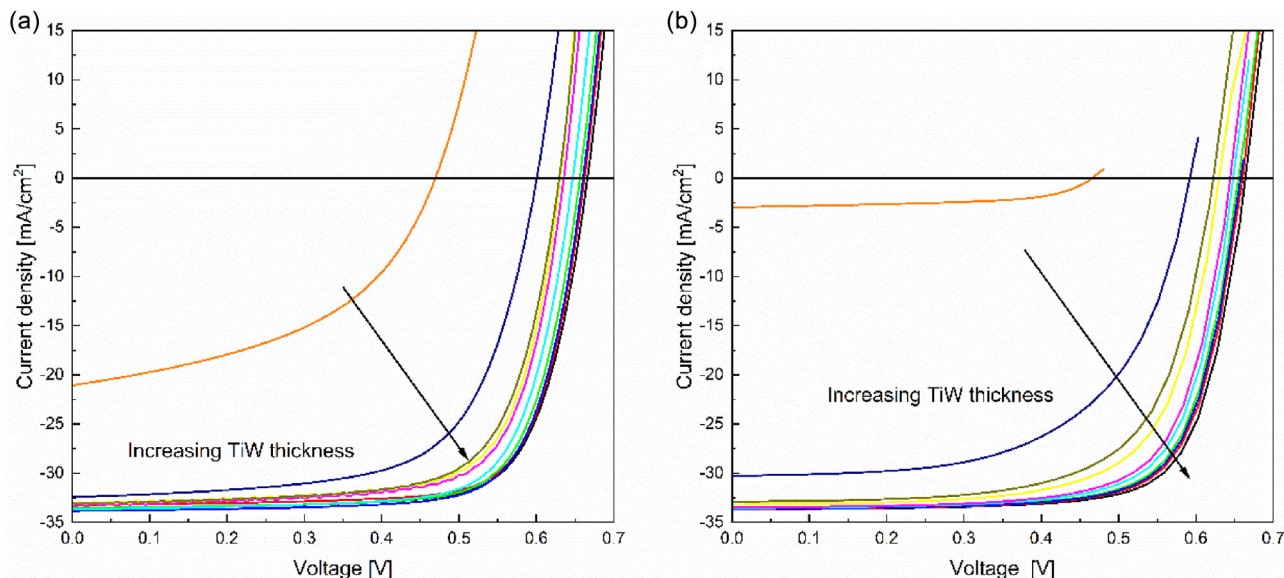


**FIGURE 4** | jV of highest performing pixels with composition SS/TiW/MoNa/Mo/CIGS/In<sub>2</sub>S<sub>3</sub>/ Window layer/ITO for different thicknesses of diffusion barrier layer as obtained through (a) experiment and (b) via SCAPS-1D.

factor (FF) with increasing thickness of barrier layer is observed. The overall comparison of  $V_{OC}$ ,  $J_{SC}$  and FF is highlighted in Table 1. The decreasing  $V_{OC}$  and  $J_{SC}$  for the CIGS cells as we go thinner in the diffusion barrier layer thickness can be explained by increased nonradiative recombination which deteriorates the quantum efficiency (Figure S5). We see a saturated collection of photons for thicker TiW films (thickness > 128 nm) below which the EQE spectra start decreasing and is strongly decreased for a no-TiW film. The increased recombination can be explained by deep level defects induced by, e.g., Fe impurities [37, 43], but from the SIMS data an additional influence of Ni and Cr cannot be excluded, which also act as recombination centers. The impact of these defect levels in reducing both the carrier lifetime and diffusion length, leading to a reduced collection efficiency has been studied earlier by others [16, 25, 36, 40]. We simulated jV for the reference 128 nm TiW barrier layer using SCAPS-1D. The material parameters are taken from the previous

**TABLE 1** | Highest performing small area pixel solar cells with different diffusion barrier thickness. The  $J_{SC}$  shown below is the  $J_{SC,exp}$  multiplied with the correction factor  $J_{SC,jv}/J_{SC,EQE}$ .

Thickness (nm)	$J_{SC}$ (mA cm <sup>-2</sup> )	$V_{OC}$ (V)	FF (%)	$\eta_{EQE}$ (%)
232	33.56	0.665	74.6	16.6
208	33.24	0.660	75.2	16.5
160	33.5	0.655	74.8	16.4
128	33.83	0.660	74.5	16.6
112	33.67	0.645	74.0	16.1
83	33.6	0.645	73.1	15.8
74	33.1	0.631	72.1	15.1
64	33.5	0.630	71.9	15.2
16	32.4	0.600	65.5	12.7
0	21.1	0.470	46.6	4.6

studies with similar composition [28, 33, 44] and listed in Table S1. Though from Figure S3 and Figure 3a, we do see a considerable concentration of Ni (in the range of  $10^{15}$ – $10^{16}$ ) and Cr (in the range of  $10^{16}$ – $10^{17}$ ) in the absorber layer, we have not included those in our analysis due to sparsely and inconsistent data available in the literature. Moreover due to their amphoteric nature, it is also difficult to predict the electronic properties of the films doped with Cr and Ni [40]. The TiW thickness is thus modeled as the Fe defect concentration (Defect III) in the SCAPS simulations (Table S1) and the concentration value for simulating 128 nm experimental curve was taken from the SIMS data. For the TiW thicknesses where the Fe concentration was not available, an estimate of the concentration was made to fit the experimental  $V_{OC}$ . The simulated  $V_{OC}$ ,  $J_{SC}$ , FF, and  $\eta$  for the 128 nm TiW with these parameters were 0.658 V, 33.6 mAcm<sup>-2</sup>, 74.08, and 16.4% respectively, which aligns well with the experimental jV parameters for 128 nm TiW. Keeping rest of the parameters the same, we varied only the defect concentrations accounting for the varying Fe concentration, and the resultant curves are shown in Figure 4b. The resultant jV parameters from the simulations are summarized in Table S2. For thickness below 74 nm, the experimental and simulations curve starts to differ in terms of  $J_{SC}$  and FF which is more prominent for a 0 nm TiW.

These results indicate that the jV<sub>SCAPS</sub> follow the jV<sub>experimental</sub> trend with respect to the change in  $V_{OC}$ ,  $J_{SC}$ , FF, and efficiency as the thickness of the barrier layer is increased. They highlight the importance of a diffusion barrier layer in controlling the diffusion of harmful impurities. As mentioned above, we only considered Fe defect concentration of a representative transition metal impurity due to limited experimental data for Cr and Ni. This simplification surely underestimates the total recombination, as Cr and Ni are also known to introduce deep state defects, possibly near mid-gap, and thus we see slightly better simulation results compared to the experimental results, especially for thicker TiW devices. For a no-TiW film, we could not reproduce entirely the experimental result even after using

a very high Fe defect concentration of the order of  $10^{21} \text{ cm}^{-3}$ . For completing the analysis, average performance of all the full area cells and the pixel cells for similar TiW thickness is summarized in Figure S6, which shows the saturation of the device's performance beyond 128 nm. While the results exhibit 128 nm to be a suitable TiW thickness, however, to maintain production-level uniformity (at both cell level and module level), mechanical durability and lifetime stability of the modules, Midsummer uses 208 nm thick TiW in their production line. This window of thickness gives a safety margin in avoiding the local failures such as pinholes and edge defects that can lead to performance losses in the modules.

## 4 | Conclusion

To summarize, the paper presents a study on using TiW as an effective barrier layer for Fe, Cr, and Ni in all-sputtered Cd-free CIGS solar cell fabricated on a steel substrate. As shown in previous studies and here also, the impact of these impurities diffusing from a substrate can have a detrimental impact on the CIGS performance. This diffusion can be reduced by increasing the thickness of the diffusion barrier layer. A barrier layer of thickness  $\approx 80 \text{ nm}$  is required to effectively screen these critical impurities from the absorber layer; however, it is for the thickness of 128 nm that the barrier layer can keep the concentration to a minimum ( $\approx 0.5 \text{ ppm}$ ). Although 128 nm TiW layer was found to be optimal to reach a high efficiency, by maintaining an effective screening of the impurities, however, for industrial production line at Midsummer a higher thickness of 208 nm is utilized which gives a CIGS solar cell with  $>16\%$  efficiency. Implementing an enhanced thickness of TiW, especially for full cells used in PV modules in an industrial setup, has proven beneficial in terms of controlling interfacial diffusion and improving the device's stability besides enhancing the module lifetime and reliability.

We studied the impact of defect concentration on the device's performance using SCAPS-1D, which correlates well with the experimental jV data of the devices. This provides an insightful perspective where just incorporating Fe defects states isn't sufficient as it may lead to underestimation of the recombination losses within a sample due to other elemental impurities. This study, combining i) SIMS, ii) experimental results on industrially relevant solar cells, and iii) simulations, suggests the possibility of exploring the impact of impurities in the future.

## Acknowledgments

This work was supported by the Wallenberg Initiative Materials Science for Sustainability (WISE) funded by the Knut and Alice Wallenberg Foundation. T.U. would like to acknowledge Johan Oliv, Klara Takei, process- and the management team at Midsummer AB and Adam Hultqvist from Angstrom Laboratory, Uppsala University. The authors gratefully acknowledge the support from ereprof. Dr. ir. Mark Burgelman, University of Gent, who supplied a reference SCAPS definition file.

## Conflicts of Interest

The authors declare no conflicts of interest.

## Data Availability Statement

The data that support the findings of this study are available in the supplementary material of this article.

## References

1. M. A. Green, E. D. Dunlop, J. Hohl-Ebinger, et al., "Cell Efficiency Tables (Version 60)," *Progress in Photovoltaics: Research and Applications* 30, no. 7 (2022): 687–701, <https://doi.org/10.1002/pip.3595>.
2. A. Wang, M. He, M. A. Green, K. Sun, and X. Hao, "A Critical Review on the Progress of Kesterite Solar Cells: Current Strategies and Insights," *Advanced Energy Materials* 13, no. 2 (2023): 2203046, <https://doi.org/10.1002/aenm.202203046>.
3. J. Keller, K. Kiselman, O. Donzel-Gargand, et al., "Alloying and Steep Back-Contact Gallium Grading Enabling Copper Indium Gallium Selenide Solar Cell with 23.6% Efficiency," *Nature Energy* 9, no. 4 (2024): 467–478, <https://doi.org/10.1038/s41560-024-01472-3>.
4. L. Zortea, S. Nishiwaki, T. P. Weiss, et al., "Cu(In, Ga)Se<sub>2</sub> Solar Cells on Low Cost Mild Steel Substrates," *Solar Energy* 175 (2018): 25–30, <https://doi.org/10.1016/j.solener.2017.12.057>.
5. M. Richards, "New World Record Efficiency with Flexible CIGS Solar Cell," *MiaSolé*, (2019). Accessed October 23, 2025. <https://miasole.com/new-world-record-efficiency-with-flexible-cigs-solar-cell/>.
6. S. Enkhardt, "Avancis Achieves 20.3% Efficiency in CIGS Solar Panel," *pv magazine* June 1, (2023). Accessed October 29, 2025. <https://www.pv-magazine.com/2023/06/01/avancis-achieves-20-3-efficiency-in-cigs-solar-panel/>.
7. Y. Hashimoto, T. Satoh, S. Shimakawa, and T. High Negami, "Efficiency CIGS Solar Cell on Flexible Stainless Steel," in *Proceedings of 3rd World Conference on Photovoltaic Energy Conversion, Proceedings of*, Vol. 1, Osaka, Japan, (2003), 574–577.
8. F. Kessler, D. Herrmann, and M. Powalla, "Approaches to Flexible CIGS Thin-Film Solar Cells," *Thin Solid Films* 480-481 (2005): 491–498, <https://doi.org/10.1016/j.tsf.2004.11.063>.
9. R. Carron, S. Nishiwaki, S.-C. Yang, et al., Soaking Treatments for High-Performance CIGS Solar Cells on Flexible Substrates, PREPRINT (Version 1) available at Research Square (2022), <https://doi.org/10.21203/rs.3.rs-2116168/v1>.
10. E. Niemi, J. Sterner, P. Carlsson, J. Oliv, E. Jaremalm, and S. Lindström, "All-Sputtered Flexible CIGS Cells at High Speed," in *31st European Photovoltaic Solar Energy Conference and Exhibition*, (2015), 1010–1013.
11. W. Shockley and H. J. Queisser, "Detailed Balance Limit of Efficiency of *p-n* Junction Solar Cells," *Journal of Applied Physics* 32, no. 3 (1961): 510–519, <https://doi.org/10.1063/1.1736034>.
12. P.-P. Choi, O. Cojocaru-Mirédin, R. Wuerz, and D. Raabe, "Comparative Atom Probe Study of Cu(In, Ga)Se<sub>2</sub> Thin-Film Solar Cells Deposited on Soda-Lime Glass and Mild Steel Substrates," *Journal of Applied Physics* 110, no. 12 (2011): 124513, <https://doi.org/10.1063/1.3665723>.
13. F. Pianezzi, A. Chirilă, P. Blösch, et al., "Electronic Properties of Cu(In, Ga)Se<sub>2</sub> Solar Cells on Stainless Steel Foils without Diffusion Barrier: Electronic Properties of CIGS Solar Cells," *Progress in Photovoltaics: Research and Applications* 20, no. 3 (2012): 253–259, <https://doi.org/10.1002/pip.1247>.
14. S. Hamtaei, G. Brammert, J. Poortmans, and B. Vermang, "A Review on Barrier Layers Used in Flexible Stainless-Steel Based CIGS Photovoltaic Devices," *npj Flexible Electronics* 7, no. 1 (2023): 1–12, <https://doi.org/10.1038/s41528-023-00266-z>.
15. K. Herz, A. Eicke, F. Kessler, R. Wächter, and M. Powalla, "Diffusion Barriers for CIGS Solar Cells on Metallic Substrates," *Thin Solid Films* 431-432 (2003): 392–397, [https://doi.org/10.1016/S0040-6090\(03\)00259-1](https://doi.org/10.1016/S0040-6090(03)00259-1).

16. C. Zhang, T. Qi, W. Wang, et al., "Efficiency CIGS Solar Cells on Flexible Stainless Steel Substrate with SiO<sub>2</sub> Diffusion Barrier Layer," *Solar Energy* 230 (2021): 1033–1039, <https://doi.org/10.1016/j.solener.2021.11.006>.
17. H. Kim and S. P. Cias, "Effect of Oxide Diffusion Barrier and Substrate on the Reliability of Stainless-Steel-Based CIGS Solar Cells," *Solar Energy Materials and Solar Cells* 272 (2024): 112888, <https://doi.org/10.1016/j.solmat.2024.112888>.
18. W. Li, X. Yan, W.-L. Xu, J. Long, A. G. Aberle, and S. Venkataraj, "Efficiency Improvement of CIGS Solar Cells by a Modified Rear Contact," *Solar Energy* 157 (2017): 486–495, <https://doi.org/10.1016/j.solener.2017.08.054>.
19. H.-J. Woo, W.-J. Lee, E.-K. Koh, et al., "Plasma-Enhanced Atomic Layer Deposition of TiN Thin Films as an Effective Se Diffusion Barrier for CIGS Solar Cells," *Nanomaterials* 11, no. 2 (2021): 370, <https://doi.org/10.3390/nano11020370>.
20. X. Jiang, B. Li, B. Song, et al., "Study on the Performance of Titanium Film as a Diffusion Barrier Layer for CIGS Solar-Cell Application on Stainless-Steel Substrates," *Clean Energy* 3, no. 3 (2019): 217–221, <https://doi.org/10.1093/ce/zkz014>.
21. Z. Gao, M. Zhao, D. Zhuang, et al., "Study on the Performance of Tungsten–Titanium Alloy Film as a Diffusion Barrier for Iron in a Flexible CIGS Solar Cell," *Solar Energy* 120 (2015): 357–362, <https://doi.org/10.1016/j.solener.2015.07.027>.
22. T. Ma, G. Jiang, W. Liu, and C. Zhu, "Doping Effects on the Crystalline and Electrical Properties of Cu<sub>2</sub>ZnSnSe<sub>4</sub> Thin Films," *Solar Energy* 115 (2015): 413–418, <https://doi.org/10.1016/j.solener.2015.02.033>.
23. M. Kim, "Explaining the Efficiency-Boosting Effects of Sodium on CIGS Solar Cells," *Scilight* 2020, no. 45 (2020): 451108, <https://doi.org/10.1063/1.50002495>.
24. D. Colombara, K. Conley, M. Malitckaya, H.-P. Komsa, and M. J. Puska, "The Fox and the Hound: In-Depth and in-Grain Na Doping and Ga Grading in Cu(In, Ga)Se<sub>2</sub> Solar Cells," *Journal of Materials Chemistry A* 8, no. 14 (2020): 6471–6479, <https://doi.org/10.1039/D0TA01103G>.
25. R. Wuerz, A. Eicke, F. Kessler, and F. Pianezzi, "Influence of Iron on the Performance of CIGS Thin-Film Solar Cells," *Solar Energy Materials and Solar Cells* 130 (2014): 107–117, <https://doi.org/10.1016/j.solmat.2014.06.038>.
26. D. Güttler, A. Chirila, S. Seyrling, et al., "Influence of NaF Incorporation during Cu(In, Ga)Se<sub>2</sub> Growth on Microstructure and Photovoltaic Performance," in *2010 35th IEEE Photovoltaic Specialists Conference*, (2010), 003420–003424, <https://doi.org/10.1109/PVSC.2010.5614564>.
27. M. Burgelman, K. Decock, S. Khelifi, and A. Abass, "Advanced Electrical Simulation of Thin Film Solar Cells," *Thin Solid Films* 535 (2013): 296–301, <https://doi.org/10.1016/j.tsf.2012.10.032>.
28. P. Bras, C. Frisk, A. Tempez, E. Niemi, and C. Platzer-Björkman, "Ga-Grading and Solar Cell Capacitance Simulation of an Industrial Cu(In, Ga)Se<sub>2</sub> Solar Cell Produced by an in-Line Vacuum All-Sputtering Process," *Thin Solid Films* 636 (2017): 367–374, <https://doi.org/10.1016/j.tsf.2017.06.031>.
29. O. Lundberg, M. Edoff, and L. Stolt, "The Effect of Ga-Grading in CIGS Thin Film Solar Cells," *Thin Solid Films* 480–481 (2005): 520–525, <https://doi.org/10.1016/j.tsf.2004.11.080>.
30. W. Witte, D. Abou-Ras, K. Albe, et al., "Gallium Gradients in Cu(In, Ga)Se<sub>2</sub> Thin-Film Solar Cells: Gallium Gradients in CIGS Thin-Film Solar Cells," *Progress in Photovoltaics: Research and Applications* 23, no. 6 (2015): 717–733, <https://doi.org/10.1002/pip.2485>.
31. M. Topič, F. Smole, and J. Furlan, "Band-Gap Engineering in CdS/Cu(In, Ga)Se<sub>2</sub> Solar Cells," *Journal of Applied Physics* 79, no. 11 (1996): 8537–8540, <https://doi.org/10.1063/1.362533>.
32. T. Dullweber, G. Hanna, W. Shams-Kolahi, et al., "Study of the Effect of Gallium Grading in Cu(In, Ga)Se<sub>2</sub>," *Thin Solid Films* 361–362 (2000): 478–481, [https://doi.org/10.1016/S0040-6090\(99\)00845-7](https://doi.org/10.1016/S0040-6090(99)00845-7).
33. C. Frisk, C. Platzer-Björkman, J. Olsson, et al., "Optimizing Ga-Profiles for Highly Efficient Cu(In, Ga)Se<sub>2</sub> Thin Film Solar Cells in Simple and Complex Defect Models," *Journal of Physics D: Applied Physics* 47, no. 48 (2014): 485104, <https://doi.org/10.1088/0022-3727/47/48/485104>.
34. S.-C. Yang, M. Ochoa, R. Hertwig, A. Aribia, A. N. Tiwari, and R. Carron, "Influence of Ga Back Grading on Voltage Loss in Low-Temperature Co-Evaporated Cu(In, Ga)Se<sub>2</sub> Thin Film Solar Cells," *Progress in Photovoltaics: Research and Applications* 29, no. 6 (2021): 630–637, <https://doi.org/10.1002/pip.3413>.
35. T. Eisenbarth, R. Caballero, C. A. Kaufmann, A. Eicke, and T. Unold, "Influence of Iron on Defect Concentrations and Device Performance for Cu(In, Ga)Se<sub>2</sub> Solar Cells on Stainless Steel Substrates," *Progress in Photovoltaics: Research and Applications* 20, no. 5 (2012): 568–574, <https://doi.org/10.1002/pip.2260>.
36. Z. Ma, D. Gao, J. Zhang, et al., "Traces of Iron Impurities in Copper Sources Can Be a Poison to Cu(In, Ga)Se<sub>2</sub> Solar Cells," *Nano Select* 3, no. 6 (2022): 1036–1041, <https://doi.org/10.1002/nano.202100296>.
37. J. Chantana, S. Teraji, T. Watanabe, and T. Minemoto, "Influences of Fe and Absorber Thickness on Photovoltaic Performances of Flexible Cu(In, Ga)Se<sub>2</sub> Solar Cell on Stainless Steel Substrate," *Solar Energy* 173 (2018): 126–131, <https://doi.org/10.1016/j.solener.2018.07.045>.
38. M. Hartmann, M. Schmidt, A. Jasenek, et al., "Flexible and Light Weight Substrates for Cu(In, Ga)Se/Sub<sub>2</sub>/ Solar Cells and Modules," in *Conference Record of the Twenty-Eighth IEEE Photovoltaic Specialists Conference - 2000 (Cat. No.00CH37036)* (2000), 638–641, <https://doi.org/10.1109/PVSC.2000.915924>.
39. S. Khelifi, A. Belghachi, J. Lauwaert, et al., "Characterization of Flexible Thin Film CIGSe Solar Cells Grown on Different Metallic Foil Substrates," *Energy Procedia* 2, no. 1 (2010): 109–117, <https://doi.org/10.1016/j.egypro.2010.07.017>.
40. F. Pianezzi, S. Nishiwaki, L. Kranz, et al., "Influence of Ni and Cr Impurities on the Electronic Properties of Cu(In, Ga)Se<sub>2</sub> Thin Film Solar Cells: Influence of Ni and Cr Impurities in CIGS," *Progress in Photovoltaics: Research and Applications* 23, no. 7 (2015): 892–900, <https://doi.org/10.1002/pip.2503>.
41. J. Rechid, R. Thyen, A. Raitzig, et al., "9% Efficiency: CIGS on Cu Substrate," in *Proceedings of 3rd World Conference on Photovoltaic Energy Conversion, Proceedings of*, Vol. 1, Osaka, Japan, (2003), pp. 559–561.
42. P. Jackson, P. Grabitz, A. Strohm, G. Bilger, and H.-W. Schock, "Contamination of Cu(In, Ga)Se<sub>2</sub> Solar Cells by Metallic Substrate Elements," in *Proceedings of the 19th European Photovoltaic Solar Energy Conference*, Paris, France, June 7–11, (2004), 1936.
43. D. Kim, K. Kim, M. Kim, and C. Jeon, "Effect of the Mo Structure on CIGS Solar Cells Fabricated on Stainless Steel Substrates," *Israel Journal of Chemistry* 55, no. 10 (2015): 1064–1069, <https://doi.org/10.1002/ijch.201400186>.
44. N. Khoshsirat and N. A. Md Yunus, "Numerical Analysis of In<sub>2</sub>S<sub>3</sub> Layer Thickness, Band Gap and Doping Density for Effective Performance of a CIGS Solar Cell Using SCAPS," *Journal of Electronic Materials* 45, no. 11 (2016): 5721–5727, <https://doi.org/10.1007/s11664-016-4744-6>.

## Supporting Information

Additional supporting information can be found online in the Supporting Information section. **Supporting Fig. 1:** GDOES data for the CIGS cells with varying TiW thickness. **Supporting Fig. 2:** GDOES data showing the diffusion of Fe and Cr through different thickness of TiW. While the signal is quite weak, a prominent (relative to other thickness) Fe signal intensity is still observed for 0 nm TiW in the absorber layer. The Cr

signal remains the same for the three thicknesses within the absorber layer. **Supporting Fig. 3:** Cr (a) and Ni (b) concentration in CIGS cell obtained through SIMS measured at the center shows decreasing diffusion of the impurity with increasing thickness of the barrier layer (128 nm, 112 nm, 83 nm, 74 nm, and 64 nm). **Supporting Fig. 4:** jV of highest performing pixels with composition SS/TiW/MoNa/Mo/CIGS/In<sub>2</sub>S<sub>3</sub>/ Window layer/ITO for a different thickness of diffusion barrier layer. **Supporting Fig. 5:** QE of CIGS solar cell with composition SS/TiW/MoNa/Mo/CIGS/In<sub>2</sub>S<sub>3</sub>/Window layer/ITO (a) with different diffusion barrier thickness and (b) 128 nm TiW simulated via SCAPS 1D (line). **Supporting Fig. 6:** Comparison of the average  $V_{OC}$ , FF, and efficiency of the full area CIGS and pixel cells of the same thickness. The standard (reference) TiW is shown in red symbol. **Supporting Table 1:** parameters used for SCAPS 1D modeling. **Supporting Table 2:** jV parameters obtained from SCAPS-1D simulation.